Bacteriorhodopsin/Ag Nanoparticle-Based Hybrid Nano-Bio Electrocatalyst for Efficient and Robust H 2 Evolution from Water

ARTICLE *in* JOURNAL OF THE AMERICAN CHEMICAL SOCIETY · FEBRUARY 2015

Impact Factor: 12.11 · DOI: 10.1021/jacs.5b00200 · Source: PubMed

JACS
JOURNAL OF THE AMERICAN CHEMICAL SOCIETY

Communication

pubs.acs.org/JACS

Bacteriorhodopsin/Ag Nanoparticle-Based Hybrid Nano-Bio Electrocatalyst for Efficient and Robust H_2 Evolution from Water

Zhenlu Zhao,[†,‡] Ping Wang,[†] Xiaolong Xu,[†] Mordechai Sheves,[§] and Yongdong Jin*[,†]

[†]State Key Lab of Electroanalytical Chemistry, Changchun Institute of Applied Chemistry, Chinese Academy of Sciences, No. 5625 Renming Street, Changchun 130022, Jilin China

[‡]Graduate School of the Chinese Academy of Sciences, Beijing 100049, China

[§]Department of Organic Chemistry, Weizmann Institute of Science, Rehovot 76100, Israel

Supporting Information

ABSTRACT: Searching for novel hybrid electrocatalysts with high activity and strong durability for a direct electrochemical hydrogen evolution reaction (HER) is extremely desirable but still remains a significant challenge. Herein, we report a novel solid carbon cloth-supported hybrid nano-bio electrocatalyst, decorated with Ag nanoparticles and proton-pumping bacteriorhodopsin (bR) (Ag/bR/CP) that were prepared by in situ electroless deposition and vesicle fusion technology, respectively. When applied as a hydrogen evolution cathode, the Ag/bR/CP shows a low onset overpotential of 63 mV, good durability (no detectable change in its catalytic activity for up to 1000 cycles in alkaline media), and enhanced HER performance under 550 nm irradiation, attributed to the activation of Ag and synergistic effects following light absorption, demonstrated by photoelectrochemical measurements.

Electrochemical water reduction for hydrogen, an energy carrier for sustainable energy applications,[1] offers promising strategies to address the escalating global energy demand. To achieve efficient water splitting, active catalysts for hydrogen evolution reaction (HER) are required.[2] Although Pt-based catalysts exhibit high HER catalytic performance, they are not suitable for large-scale practical applications because of their high costs and the scarcity of Pt.[3] Abundant nickel-based alloys are also commercially used as HER catalysts, but they are not stable enough to operate in acidic environments.[4] The limitations of precious HER catalysts have motivated the search and development of non-Pt catalysts. Several non-Pt metal nanomaterials, such as transition metal nitrides,[5] carbides,[6] sulfides,[7] borides,[8] phosphides,[9] and composites,[10] along with metal alloys,[11] have been intensively investigated as catalysts for hydrogen evolution from water.[12] In addition, recent research has shown active carbon-based catalysts[13] and metal-based molecular catalysts[14] to be efficient hydrogen evolving catalysts. Despite recent great progress in the development of various catalysts to facilitate the HER, developing novel HER materials and improving strategies to further prompt HER remains a great challenge.

Bacteriorhodopsin (bR), a proton-pumping protein in the purple membrane of *Halobacterium salinarum*,[15] due to its exceptional stability toward thermal, chemical, and photochemical degradation and unique photoelectric and photochromic properties, has aroused research interest toward solar energy conversion applications.[16] Notably, while in the majority of reports bR was considered as a proton pump and electron transporter,[16,17] there is no report so far on the use of bR as an active component in electrocatalytic water splitting for HER.

Herein, we exploit bR, for the first time, as an active component for electrochemical HER application by electroless deposition of Ag nanoparticles (AgNPs) on top of solid carbon cloth-supported bR monolayers, denoted as Ag/bR/CP, and CP represents carbon cloth with poly(diallyldimethylammonium chloride) (PDDA) functionalization. When used as a robust integrated hydrogen-evolving cathode, the Ag/bR/CP electrode behaves like an n-type semiconductor and shows excellent activity, stability, and enhanced HER activity under irradiation because of synergistic effects between AgNP and bR. With pH increase from 3 to 10, the Ag/bR/CP electrode shows enhanced HER performance. In alkaline media, the Ag/bR/CP electrode shows a low onset overpotential of only 63 mV and needs overpotentials of 84 and 350 mV to drive current densities of 1 and 10 mA cm^{-2}, respectively, much lower than that of other reported non-Pt HER catalysts.

The Ag/bR/CP electrode was fabricated by in situ electroless deposition of AgNPs on top of the solid carbon cloth-supported bR monolayers.[18] The carbon cloth-supported bR monolayers were prepared according to our previously developed method[15b] by adsorbing freshly prepared phosphatidylcholine unilamellar vesicles with incorporated wild-type bR (bR-vesicles) on all accessible surfaces of fibrous carbon cloth substrate and their fusion into random monolayers. The mean hydrodynamic size of the parent bR-vesicles determined by dynamic light scattering is about 80 nm, and the vesicle suspension displays typical bR absorption at about 568 nm (Figure S1, Supporting Information (SI)). To promote electrostatic adsorption of the surface negatively charged bR-vesicles onto the substrate, prior to use the carbon cloth was functionalized by PDDA to obtain a positively charged surface. bR proteins prepared by vesicle fusion tactics[15b] are supposed to be well oriented on the fiber surfaces of the carbon cloth. Figure S2 (SI) shows the N and Cl X-ray photoelectron

Received: January 8, 2015
Published: February 15, 2015

DOI: 10.1021/jacs.5b00200
J. Am. Chem. Soc. 2015, 137, 2840−2843

spectroscopy (XPS), in which the principal peaks at around 400 and 198.5 eV could be ascribed to the binding energies of the N 1s and Cl 2p,[19] indicating the functionalization of carbon cloth with PDDA (denoted as CP thereafter). The scanning electron microscopy (SEM) images and energy-dispersive X-ray spectroscopy (EDX) analyses (Figures S3 (SI)) further confirmed the formation of CP. After bR deposition by vesicle fusion, the resulting bR/CP displays a distinct UV−vis absorption peak at ∼568 nm (Figure S4 (SI)), the characteristic of bR absorption. Furthermore, the peaks observed at 134 and 163 eV in the P 2p and S 2p XPS spectra (Figure S5 (SI)) indicate the presence of P and S in the as-synthesized bR/CP. The SEM images and corresponding EDX elemental mapping images shown in Figure S6 (SI) further show that both P and S elements that originated from bR proteins are uniformly distributed on the surface of the bR/CP, verifying successful coating of bR monolayers onto CP.

Figure 1a−c show typical SEM and transmission electron microscopy (TEM) images of the final Ag-deposited Ag/bR/CP, indicating successful uniform deposition of small AgNPs (with mean diameter of ∼8 nm) on the bR/CP surface. The UV−vis absorption spectrum of the Ag/bR/CP in Figure S4 (SI) shows a typical AgNP plasmon band and bR absorption peak at 422 and 568 nm, respectively. The XPS spectrum of the as-prepared Ag/bR/CP was further investigated (Figure S7 (SI)). Two characteristic peaks arising from Ag $3d_{5/2}$ and Ag $3d_{3/2}$ orbitals are located at 368.3 and 374.3 eV (Figure S7b (SI)), suggesting that Ag is mainly present in the metallic state.[20] To get further insight into the distribution of Ag and bR, elemental analysis was carried out with scanning transmission electron microscopy (STEM). Figure 1d−h and Figure S8 (SI) (with higher scale images) show high-angle annular dark-field (HAADF) micrograph and elemental maps of Ag, P, S, and N of a selected area of the Ag/bR/CP, further demonstrating the successful preparation and uniformity of the Ag/bR/CP heterostructures.

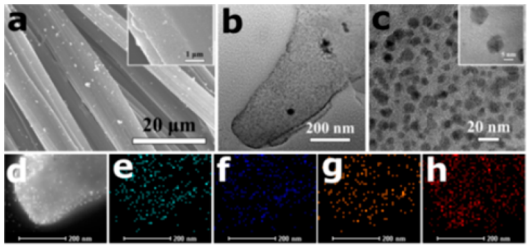

Figure 1. Low- and high-magnification SEM (a) and TEM (b,c) images of the Ag/bR/CP. HAADF STEM (d) image of the Ag/bR/CP, and corresponding elemental mapping for Ag (e), P (f), S (g), and N (h). (Scale bar in (d−h): 200 nm).

For comparison, bR-free small AgNP-decorated CP heterostructures (Ag/CP) were also prepared via electroless metal deposition by using the same procedures under identical conditions and thoroughly demonstrated by UV−vis absorption spectrum (Figure S4 (SI)), SEM images and EDX analyses (Figure S9 (SI)), TEM images (Figure S10 (SI)), and XPS spectra (Figure S11 (SI)). The amount of Ag in the Ag/CP and Ag/bR/CP is nearly 1:1, determined by inductively coupled plasma mass spectrometry (ICP-MS) measurements.

Figure 2a shows the polarization curve of the Ag/CP, bR/CP, and Ag/bR/CP cathodes, respectively, before and after light irradiation in 1.0 M PBS (pH 10) with a scan rate of 2 mV s^{-1}. Notably, as compared to the control Ag/CP and bR/CP electrodes, the Ag/bR/CP shows significantly high HER activity with greater current over the whole potential range and lower onset overpotential (cf. Table S1 and Figure S12 (SI)). Also, the bR/CP electrode displays a weaker but still considerable HER activity in the dark. These imply that bR acts as an active catalyst component (other than proton pumping capability) for electrochemical HER and the existence of synergistic effects of bR and AgNPs for enhanced HER performance. The onset overpotential of the Ag/bR/CP is as low as 63 mV under light irradiation, which is much lower than that of Ag/CP (Table S1 (SI)). When recorded at −0.3, −0.4, and −0.5 V, respectively, the HER current densities of the Ag/bR/CP are all about 2.3 times as high as that of the Ag/CP (cf. Figure S12b (SI)). In addition, this electrode needs an overpotential of only 84 and 350 mV to drive current density of 1 and 10 mA cm^{-2}, respectively. These overpotentials compare favorably to or even surpass those of recently reported advanced non-Pt HER catalysts in alkaline media (Table S2 (SI)). Moreover, all three samples showed small but detectable enhanced HER activity under light irradiation. As shown in Figure S13 (SI), the current density of the Ag/bR/CP electrode, after normalization to the electrochemically active surface area (ECSA) obtained by Ag underpotential deposition experiments, is still obviously higher than that of the Ag/CP and bR/CP electrodes in the HER potential region, further indicating that the change in the onset for H_2 evolution is a kinetic effect rather than a simple surface effect in the system. The enhanced HER activity under light irradiation may be

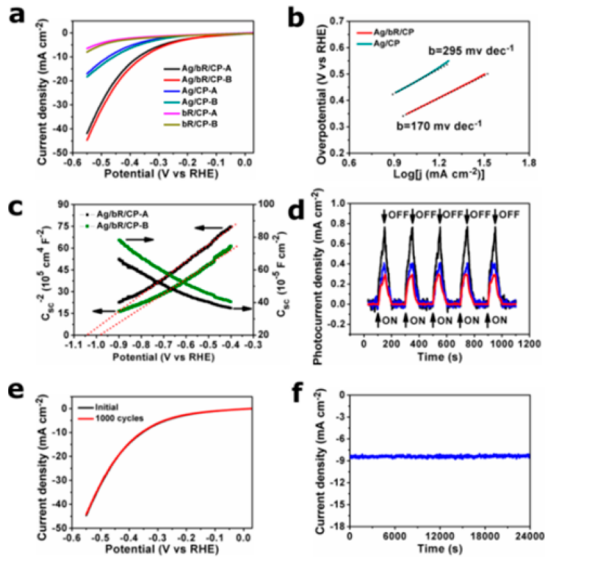

Figure 2. (a) Polarization curves of the Ag/CP, bR/CP, and Ag/bR/CP electrodes before (denoted with -A) and after (denoted with -B) light irradiation with a scan rate of 2 mV s^{-1}. (b) Tafel plot of the Ag/CP and Ag/bR/CP electrodes after light irradiation. (c) Series capacitances as a function of the electrode potential and Mott−Schottky plots for Ag/bR/CP before (-A) and after (-B) light irradiation at 1 kHz frequencies. (d) Normalized photocurrent responses of the Ag/CP (blue), bR/CP (red), and Ag/bR/CP (black), respectively, at −300 mV (vs RHE). (e) Polarization curves of the Ag/bR/CP electrode obtained initially and after 1000 CV scans under irradiation. (f) Time-dependent current density curve for the Ag/bR/CP electrode under static overpotential of 350 mV for 24000 s. All the measurements were tested in O_2-purged 1.0 M PBS (pH 10) at room temperature.

DOI: 10.1021/jacs.5b00200
J. Am. Chem. Soc. 2015, 137, 2840−2843

attributed mainly to the surface activation of Ag and synergistic effects between Ag and bR.

To further evaluate the catalytic reaction efficiency of the Ag/bR/CP electrode, the catalytic kinetics of the Ag/bR/CP and control Ag/CP and bR/CP electrodes were examined. First, electrical impedance spectroscopy (EIS) was performed (Figure S14 (SI)). As compared to Ag/CP and bR/CP, the Ag/bR/CP shows a low charge transfer resistance in the high frequency region of the Nyquist plot, indicative of favorable charge transport kinetics. The higher electroconductivity of the Ag/bR/CP electrode was believed to play a crucial role in enhancing its electrochemical performance. In addition, Tafel plots as shown in Figure 2b are considered with the linear regions fitted into the Tafel equation. The Ag/bR/CP electrode exhibits a Tafel slope of ~170 mV dec^{-1} in the region of η = 350−500 mV, revealing that the rate-determining step of the HER process is electrochemical hydrogen adsorption in this hybrid nanosystem.[21] In comparison with the Tafel slope of Ag/CP (295 mV dec^{-1}), the Ag/bR/CP displays a lower Tafel slope, which further manifests the enhanced kinetics of the Ag/bR/CP. The value of exchange current density of Ag/bR/CP is calculated to be 586 μA cm^{-2} by extrapolating the Tafel plot (Figure S15 (SI)), which is larger than that of Ag/CP (341 μA cm^{-2}). Such high catalytic performance of the Ag/bR/CP, obviously better than its single compoments, could be ascribed to the synergistic effects from bR and AgNPs; in this hybrid nanosystem, bR provides its biological function of pumping protons to the H_2-evolving Ag cocatalyst following light absorption, prompting the adsorption and formation of Ag−$H_{adsorption}$ on AgNP surfaces, which accelerates the rate-determining step of the HER process (electrochemical hydrogen adsorption)[21] and therefore results in enhanced evolution of hydrogen (Scheme S1 (SI)).

To further study the synergistic effect and mechanisms of the materials for HER, photoelectrochemical measurements were carried out using the typical three-electrode system. Potentiodynamic electrochemical impedance spectroscopy was performed for bR/CP and Ag/bR/CP at 1 kHz frequency. The capacitances vs potential and Mott−Schottky plots of the Ag/bR/CP and bR/CP are presented in Figure 2c and Figure S16 (SI). Both Ag/bR/CP and bR/CP electrodes demonstrated positive slopes in the Mott−Schottky plots, indicating that the Ag/bR/CP and bR/CP behave like an n-type semiconductor.[22] Notably, the Ag/bR/CP shows smaller slope of the Mott−Schottky plot compared to bR/CP, suggesting a faster charge transfer (Table S3 (SI)). The calculated carrier densities (N_D) of the Ag/bR/CP and bR/CP under light irradiation enlarged and were 1.79×10^{23} and 6.80×10^{22} cm^{-3}, respectively. The higher N_D of the Ag/bR/CP signified a faster carrier transfer and thus enhanced photoelectrochemical water splitting property.[23]

For a conventional n-type semiconductor, such as TiO_2 or a TiO_2−Au system, a negative shift in the Fermi level of the TiO_2 would occur if electrons accumulate in the TiO_2 or TiO_2−Au system under irradiation because the Fermi level is directly related to the number of accumulated electrons and the electron accumulation increases the Fermi level of Au to more negative potentials.[24] However, we found that the flat-band potential of Ag/bR/CP (−0.98 V vs RHE) is more anodic than that of bR/CP (−1.08 V vs RHE) under light irradiation in our system by comparing the Mott−Schottky plots of the Ag/bR/CP and bR/CP that presented in Figure 2c and Figure S16 (SI). This result indicated that the Fermi level of the AgNP/bR nanohybrid, behaving like an n-type semiconductor, shifts to more positive potentials when irradiated (Figure S17 (SI)). This shift is tentatively attributed to the accumulation of protons and hence increased carrier densities that caused synergistically by bR and AgNPs with strong reduction performance under alkaline condition during the process.

Figure 2d shows the normalized photocurrent responses of Ag/CP, bR/CP and Ag/bR/CP under light illumination. As shown in Table S4 (SI), the photocurrent of the bare bR/CP is ~305 μA cm^{-2}, while the current of Ag/CP is 415 μA cm^{-2} at −300 mV vs RHE. In the case of the Ag/bR/CP, the photocurrent reaches a value of 773 μA cm^{-2}, which is 7.4% higher than that of the sum of bare bR/CP and Ag/CP. This result further indicated synergism between AgNP and bR, which enhances the HER properties of the hybrid catalyst.

We further examined the durability of the Ag/bR/CP electrode. The polarization curve shows negligible difference after 1000 cycles, suggesting superior stability of the Ag/bR/CP in the long-term electrochemical process (Figure 2e). The time-dependent current density curve at −400 mV (vs RHE) suggests that the as-prepared Ag/bR/CP electrode maintains its catalytic activity for at least 24000 s (Figure 2f).

We also further investigated the HER performance of the Ag/bR/CP in 1.0 M PBS at pH's 3 and 7, respectively. In either acidic or neutral conditions, the HER performance of the electrodes demonstrated the same tendency. The Ag/bR/CP showed more favorable HER activity than Ag/CP, and the Ag/bR/CP showed enhanced HER activity under irradiation and excellent durability (Figure 3 and Figure S18 (SI)). The onset

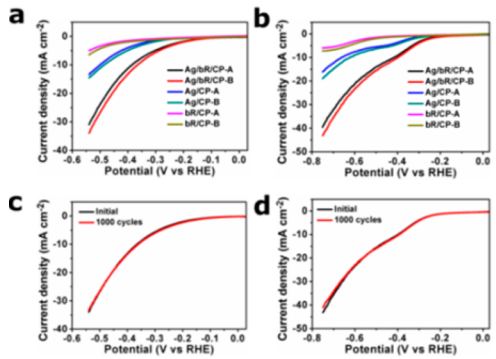

Figure 3. Polarization curves of the Ag/CP, bR/CP, and Ag/bR/CP electrodes before (-A) and after (-B) light irradiation at pH 7 (a) and pH 3 (b). Polarization curves of the Ag/bR/CP recorded initially and after 1000 CV scans at pH 7 (c) and pH 3 (d) under irradiation. All the measurements were performed in O_2-purged 1.0 M PBS with a scan rate of 2 mV s^{-1} at room temperature.

overpotential of the Ag/bR/CP electrode under light irradiation is only 76 mV in neutral conditions, and this electrode needs overpotentials of 199 and 364 mV to drive current densities of 2 and 10 mA cm^{-2}, respectively, much lower than that required by other reported non-Pt HER catalysts in neutral media (Table S5 (SI)). As shown in Figure 3b,d, unlike those at pH 7, the HER polarization curves at pH 3 display two reduction waves, with a shoulder peak around −0.4 V. This is supposed to be related with a strong adsorption of hydronium ion (H_3O^+) on catalyst surface in acidic media, followed by electrochemical reduction into adsorbed H and the formation of adsorbed H to H_2.[25] With pH increase from 3 to 10, the onset overpotential and Tafel slope of Ag/bR/CP

DOI: 10.1021/jacs.5b00200
J. Am. Chem. Soc. 2015, 137, 2840−2843

electrode becomes smaller and smaller (Table S1, Figure S19a,b (SI)), revealing that Ag/bR/CP showed enhanced HER performance. Table S4, Figure S19c,d (SI) showed the normalized photocurrent density of the bR/CP, Ag/CP, and Ag/bR/CP under different pH at −300 mV (vs RHE), further exhibiting enhanced HER performance, which is related with strong reduction performance of AgNPs under alkaline condition and synergistic effects between AgNP and bR.

In summary, a hybrid nano-bio electrocatalyst material, Ag/bR/CP, was prepared successful by in situ electroless deposition of Ag nanoparticles on top of the solid carbon cloth-supported bR and exploited for direct electrochemical hydrogen evolution. The Ag/bR/CP electrode displays excellent catalytic performance, good stability, and enhanced HER activity under light irradiation, induced by the strong reduction performance of AgNPs and the interaction between the AgNP and bR. This study provides promising features for the design of novel hybrid catalysts with improved activity and durability for many other areas, such as solar cell, metal−air batteries, and supercapacitors.

■ ASSOCIATED CONTENT

Supporting Information

Experimental details, additional characterizations, and supplementary results and discussion. This material is available free of charge via the Internet at http://pubs.acs.org.

■ AUTHOR INFORMATION

Corresponding Author

*ydjin@ciac.ac.cn.

Notes

The authors declare no competing financial interest.

■ ACKNOWLEDGMENTS

This work was supported by the National Natural Science Foundation of China (grant 21475125), and the Hundred Talents Program of the Chinese Academy of Sciences. We thank the Weizmann Institute of Science for a Feinberg Foundation Visiting Faculty Fellowship.

■ REFERENCES

(1) Turner, J. A. *Science* **2004**, *305*, 972.

(2) Morales-Guio, C. G.; Stern, L.-A.; Hu, X. *Chem. Soc. Rev.* **2014**, *43*, 6555.

(3) Sheng, W.; Gasteiger, H. A.; Shao-Horn, Y. *J. Electrochem. Soc.* **2010**, *157*, B1529.

(4) Raj, I. A.; Vasu, K. I. *J. Appl. Electrochem.* **1990**, *20*, 32.

(5) Cao, B.; Veith, G. M.; Neuefeind, J. C.; Adzic, R. R.; Khalifah, P. G. *J. Am. Chem. Soc.* **2013**, *135*, 19186.

(6) (a) Zhao, Y.; Kamiya, K.; Hashimoto, K.; Nakanishi, S. *Angew. Chem., Int. Ed.* **2013**, *52*, 13638. (b) Chen, W. F.; Wang, C. H.; Sasaki, K.; Marinkovic, N.; Xu, W.; Muckerman, J. T.; Zhu, Y.; Adzic, R. R. *Energy Environ. Sci.* **2013**, *6*, 943. (c) Wan, C.; Regmi, Y. N.; Leonard, B. M. *Angew. Chem., Int. Ed.* **2014**, *53*, 6407.

(7) (a) Kibsgaard, J.; Chen, Z.; Reinecke, B. N.; Jaramillo, T. F. *Nature Mater.* **2012**, *11*, 963. (b) Cheng, L.; Huang, W.; Gong, Q.; Liu, C.; Liu, Z.; Li, Y.; Dai, H. *Angew. Chem., Int. Ed.* **2014**, *53*, 7860. (c) Vrubel, H.; Merki, D.; Hu, X. *Energy Environ. Sci.* **2012**, *5*, 6136. (d) Ding, Q.; Meng, F.; English, C. R.; Shearer, M. J.; Liang, D.; Daniel, A. S.; Hamers, R. J.; Jin, S. *J. Am. Chem. Soc.* **2014**, *136*, 8504. (e) Huang, X.; Zeng, Z.; Bao, S.; Wang, M.; Qi, X.; Fan, Z.; Zhang, H. *Nature Commun.* **2013**, *4*, 1444. (f) Sun, Y.; Liu, C.; Grauer, D. C.; Yano, J.; Long, J. R.; Yang, P.; Chang, C. J. *J. Am. Chem. Soc.* **2013**, *135*, 17699.

(8) Vrubel, H.; Hu, X. *Angew. Chem., Int. Ed.* **2012**, *51*, 12703.

(9) (a) Popczun, E. J.; Read, C. G.; Roske, C. W.; Lewis, N. S.; Schaak, R. E. *Angew. Chem., Int. Ed.* **2014**, *53*, 5427. (b) Popczun, E. J.; McKone, J. R.; Read, C. G.; Biacchi, A. J.; Wiltrout, A. M.; Lewis, N. S.; Schaak, R. E. *J. Am. Chem. Soc.* **2013**, *135*, 9267. (c) Kibsgaard, J.; Jaramillo, T. F. *Angew. Chem., Int. Ed.* **2014**, *53*, 14433.

(10) (a) Wang, H.; Lu, Z.; Kong, D.; Sun, J.; Hymel, T. M.; Cui, Y. *ACS Nano* **2014**, *8*, 4940. (b) Kong, D.; Wang, H.; Lu, Z.; Cui, Y. *J. Am. Chem. Soc.* **2014**, *136*, 4897. (c) Gong, M.; Zhou, W.; Tsai, M.-C.; Zhou, J.; Guan, M.; Lin, M.-C.; Zhang, B.; Hu, Y.; Wang, D.-Y.; Yang, J.; Pennycook, S. J.; Hwang, B.-J.; Dai, H. *Nature Commun.* **2014**, *5*, 4695. (d) Zou, X.; Huang, X.; Goswami, A.; Silva, R.; Sathe, B. R.; Mikmeková, E.; Asefa, T. *Angew. Chem., Int. Ed.* **2014**, *53*, 4372.

(11) Danilovic, N.; Subbaraman, R.; Strmcnik, D.; Chang, K.-C.; Paulikas, A. P.; Stamenkovic, V. R.; Markovic, N. M. *Angew. Chem., Int. Ed.* **2012**, *51*, 12495.

(12) Subbaraman, R.; Tripkovic, D.; Chang, K.-C.; Strmcnik, D.; Paulikas, A. P.; Hirunsit, P.; Chan, M.; Greeley, J.; Stamenkovic, V.; Markovic, N. M. *Nature Mater.* **2012**, *11*, 550.

(13) (a) Zheng, Y.; Jiao, Y.; Zhu, Y.; Li, L. H.; Han, Y.; Chen, Y.; Du, A.; Jaroniec, M.; Qiao, S. Z. *Nature Commun.* **2014**, *5*, 3783. (b) Shalom, M.; Gimenez, S.; Schipper, F.; Herraiz-Cardona, I.; Bisquert, J.; Antonietti, M. *Angew. Chem., Int. Ed.* **2014**, *53*, 3654.

(14) (a) McKone, J. R.; Marinescu, S. C.; Brunschwig, B. S.; Winkler, J. R.; Gray, H. B. *Chem. Sci.* **2014**, *5*, 865. (b) Kleingardner, J. G.; Kandemir, B.; Bren, K. L. *J. Am. Chem. Soc.* **2013**, *136*, 4. (c) Zhang, P.; Wang, M.; Yang, Y.; Yao, T.; Sun, L. *Angew. Chem., Int. Ed.* **2014**, *53*, 13803.

(15) (a) Jin, Y. D.; Honig, T.; Ron, I.; Friedman, N.; Sheves, M.; Cahen, D. *Chem. Soc. Rev.* **2008**, *37*, 2422. (b) Jin, Y. D.; Friedman, N.; Sheves, M.; He, T.; Cahen, D. *Proc. Natl. Acad. Sci. U. S. A.* **2006**, *103*, 8601.

(16) (a) Wang, P.; Dimitrijevic, N. M.; Chang, A. Y.; Schaller, R. D.; Liu, Y.; Rajh, T.; Rozhkova, E. A. *ACS Nano* **2014**, *8*, 7995. (b) Balasubramanian, S.; Wang, P.; Schaller, R. D.; Rajh, T.; Rozhkova, E. A. *Nano Lett.* **2013**, *13*, 3365. (c) Allam, N. K.; Yen, C.-W.; Near, R. D.; El-Sayed, M. A. *Energy Environ. Sci.* **2011**, *4*, 2909.

(17) (a) Biesso, A.; Qian, W.; Huang, X.; El-Sayed, M. A. *J. Am. Chem. Soc.* **2009**, *131*, 2442. (b) Yen, C.-W.; Chu, L.-K.; El-Sayed, M. A. *J. Am. Chem. Soc.* **2010**, *132*, 7250. (c) Saga, Y.; Watanabe, T.; Koyama, K.; Miyasaka, T. *J. Phys. Chem. B* **1998**, *103*, 234.

(18) Ron, I.; Friedman, N.; Cahen, D.; Sheves, M. *Small* **2008**, *4*, 2271.

(19) Yang, D. Q.; Sacher, E. *J. Phys. Chem. B* **2005**, *109*, 4481.

(20) Liu, M.; Lu, Y.; Chen, W. *Adv. Funct. Mater.* **2013**, *23*, 1289.

(21) Chen, Z.; Cummins, D.; Reinecke, B. N.; Clark, E.; Sunkara, M. K.; Jaramillo, T. F. *Nano Lett.* **2011**, *11*, 4168.

(22) Li, L. S.; Xu, T.; Zhang, Y. J.; Jin, J.; Li, T. J.; Zou, B.; Wang, J.-P. *J. Vac. Sci. Technol., A* **2001**, *19*, 1037.

(23) Wang, G.; Wang, H.; Ling, Y.; Tang, Y.; Yang, X.; Fitzmorris, R. C.; Wang, C.; Zhang, J. Z.; Li, Y. *Nano Lett.* **2011**, *11*, 3026.

(24) (a) Subramanian, V.; Wolf, E. E.; Kamat, P. V. *J. Am. Chem. Soc.* **2004**, *126*, 4943. (b) Jakob, M.; Levanon, H.; Kamat, P. V. *Nano Lett.* **2003**, *3*, 353.

(25) Laursen, A. B.; Kegnaes, S.; Dahl, S.; Chorkendorff, I. *Energy Environ. Sci.* **2012**, *5*, 5577.

DOI: 10.1021/jacs.5b00200
J. Am. Chem. Soc. 2015, 137, 2840−2843